COLLOQUIUM PAPER

Cerebral cortical folding, parcellation, and connectivity in humans, nonhuman primates, and mice

David C. Van Essen[a,1], Chad J. Donahue[a], Timothy S. Coalson[a], Henry Kennedy[b,c,d], Takuya Hayashi[e], and Matthew F. Glasser[a,f]

[a]Department of Neuroscience, Washington University School of Medicine, St. Louis, MO 63110; [b]Univ Lyon, Université Claude Bernard Lyon 1, INSERM, Stem Cell and Brain Research Institute U1208, 69500 Bron, France; [c]Institute of Neuroscience, Center for Excellence in Brain Science and Intelligence Technology, Chinese Academy of Sciences, Shanghai 200031, China; [d]Shanghai Center for Brain Science and Brain-Inspired Intelligence Technology, Shanghai 200031, China; [e]Laboratory for Brain Connectomics Imaging, RIKEN Center for Biosystems Dynamics Research, Kobe, 650-0047, Japan; and [f]Department of Radiology, Washington University School of Medicine, St. Louis, MO 63110

Edited by Tony Movshon, New York University, New York, NY, and approved November 1, 2019 (received for review August 27, 2019)

Advances in neuroimaging and neuroanatomy have yielded major insights concerning fundamental principles of cortical organization and evolution, thus speaking to how well different species serve as models for human brain function in health and disease. Here, we focus on cortical folding, parcellation, and connectivity in mice, marmosets, macaques, and humans. Cortical folding patterns vary dramatically across species, and individual variability in cortical folding increases with cortical surface area. Such issues are best analyzed using surface-based approaches that respect the topology of the cortical sheet. Many aspects of cortical organization can be revealed using 1 type of information (modality) at a time, such as maps of cortical myelin content. However, accurate delineation of the entire mosaic of cortical areas requires a multimodal approach using information about function, architecture, connectivity, and topographic organization. Comparisons across the 4 aforementioned species reveal dramatic differences in the total number and arrangement of cortical areas, particularly between rodents and primates. Hemispheric variability and bilateral asymmetry are most pronounced in humans, which we evaluated using a high-quality multimodal parcellation of hundreds of individuals. Asymmetries include modest differences in areal size but not in areal identity. Analyses of cortical connectivity using anatomical tracers reveal highly distributed connectivity and a wide range of connection weights in monkeys and mice; indirect measures using functional MRI suggest a similar pattern in humans. Altogether, a multifaceted but integrated approach to exploring cortical organization in primate and nonprimate species provides complementary advantages and perspectives.

macaque | marmoset | neuroanatomy | cerebral cortex | neuroimaging

Cerebral cortex is the dominant structure of the mammalian brain and is implicated in a wide range of sensory, motor, cognitive, and emotional functions. Despite wide variations across species in size and morphological complexity, there are fundamental commonalities in cortical structure and function across all mammals. Most notably, cerebral cortex is a thin, layered sheet of gray matter containing a mosaic of cortical areas that differ in architecture, connectivity, topography (maps of sensory or motor domains), and/or function (1, 2).

Our ability to investigate how cerebral cortex is organized and how it "works" has been greatly enhanced in recent decades by a growing arsenal of powerful and complementary experimental methods, both invasive (mainly applicable to animal models) and noninvasive (widely applicable to humans). Invasive anatomical, electrophysiological, and optical methods are available over a wide range of spatial scales (micro-, meso-, and macroscopic), and they provide a remarkably rich and diverse range of information. Many of these tools require complex genetic manipulations and hence are limited to genetically tractable species, especially the mouse but more recently also the marmoset monkey. Some invasive methods can be applied to the human brain (e.g., surgical interventions and postmortem histology), but in recent years these have been dwarfed by noninvasive methods, particularly MRI. These complementary invasive and noninvasive methods have contributed to an explosion of experimental findings pertaining to cortical structure, function, and connectivity in a number of intensively studied species. An emerging general observation is that brain circuitry, including that of cerebral cortex, is exceedingly complex by many measures and at every scale examined. Indeed, this complexity far exceeds what was generally suspected in the late 20th century, early in the modern neuroscience era.

Here, we take an evolutionary perspective that focuses on a few intensively studied species—humans, nonhuman primates, and mice—and a few general topics pertaining to cerebral cortex. These include 1) macroscopic morphology and individual variability, particularly as revealed by MRI; 2) cortical parcellation, functional organization, and bilateral symmetry; and 3) corticocortical connectivity. Connectivity is particularly fundamental but is especially challenging in humans because the methods used to infer long-distance connections are indirect and subject to errors and bias. Animal models offer promise for much-needed validation studies of the noninvasive approaches that are being used in the human brain.

Brain Size and Cortical Convolutions

Brains differ dramatically across species in size and in the complexity of cortical convolutions, illustrated in Fig. 1 for 4 primate and 2 rodent species. In terms of mass, the human brain is ∼3,800 times larger than that of the mouse, which diverged from our lineage ∼75 MYA (million years ago); it is ∼290 times larger than that of the New World marmoset monkey (divergence ∼35 MYA),

This paper results from the Arthur M. Sackler Colloquium of the National Academy of Sciences, "Using Monkey Models to Understand and Develop Treatments for Human Brain Disorders," held January 7–8, 2019, at the Arnold and Mabel Beckman Center of the National Academies of Sciences and Engineering in Irvine, CA. NAS colloquia began in 1991 and have been published in PNAS since 1995. From February 2001 through May 2019, colloquia were supported by a generous gift from The Dame Jillian and Dr. Arthur M. Sackler Foundation for the Arts, Sciences, & Humanities, in memory of Dame Sackler's husband, Arthur M. Sackler. The complete program and video recordings of most presentations are available on the NAS website at http://www.nasonline.org/using-monkey-models.

Author contributions: D.C.V.E., C.J.D., T.S.C., H.K., T.H., and M.F.G. designed research; D.C.V.E., C.J.D., T.S.C., T.H., and M.F.G. performed research; T.S.C., T.H., and M.F.G. contributed new reagents/analytic tools; D.C.V.E., C.J.D., T.S.C., H.K., T.H., and M.F.G. analyzed data; and D.C.V.E., C.J.D., T.S.C., H.K., T.H., and M.F.G. wrote the paper.

The authors declare no competing interest.

This article is a PNAS Direct Submission.

Published under the PNAS license.

Data deposition: Data reported in this study have been deposited in the BALSA database for extensively analyzed neuroimaging data at https://balsa.wustl.edu/study/976M4.

[1]To whom correspondence may be addressed. Email: vanessen@wustl.edu.

This article contains supporting information online at https://www.pnas.org/lookup/suppl/doi:10.1073/pnas.1902299116/-/DCSupplemental.

First published December 23, 2019.

NEUROSCIENCE

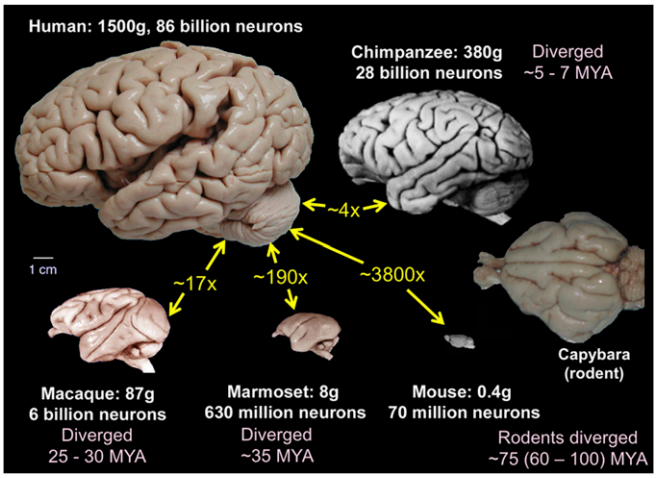

Fig. 1. Brain images of 4 primate and 2 rodent species. Size ratios (yellow text) are based on brain weight. The scale bar applies to all images. Primate and mouse brain images were adapted with permission from ref. 3. Capybara (a gyrencephalic rodent) image courtesy of Suzana Herculano-Houzel, Vanderbilt University, Nashville, TN.

~17 times larger than that of the Old World macaque monkey (divergence ~25 to 30 MYA), and 4 times larger than that of our closest living relative, the chimpanzee, which diverged 5 to 7 MYA (4–6). Human brain expansion relative to the great apes occurred mainly in the last 1 to 2 million y (7–9).

The wide range in complexity of cortical convolutions reflects well-known anatomical scaling relationships as a function of total brain size. With increasing brain size, subcortical structures (brainstem, thalamus, basal ganglia) increase more slowly in volume than does cerebral cortex (8, 10, 11). Subcortical white matter, on the other hand, increases more steeply than does cortical gray matter volume (12). However, increases in cortical volume are reflected mainly in an expanded surface area, because cortical thickness increases with a very shallow slope (13, 14). Beyond a critical brain size (~7 g), all species are gyrencephalic, with a cortical folding index >1 (14), because cortical surface area exceeds the minimum external surface area of the combined subcortical gray matter, white matter, and ventricles. Beyond this transition, cortex becomes progressively more convoluted with increases in brain size, thereby ensuring an intimate contact between cortex and the white matter it enshrouds (15). How factors other than size determine the distinctive pattern of cortical folds in any given species (or individual) is a different matter. Despite the differences in folding extent, gyrencephalic primates share many primary sulci, such as the lateral, superior temporal, and (except for the marmoset) central sulci (Fig. 1). In contrast, gyrencephalic species from other mammalian orders have very different folding patterns (e.g., capybara in Fig. 1). Insofar as cortical folds are correlated to some degree with areal boundaries (16), major differences in folding patterns may reflect differences in the areal layout in primates vs. other mammalian orders (9).

Folding Variability, Bilateral Symmetry, and Brain Atlases

Using structural MRI scans to examine cortical folding patterns in 3 gyrencephalic primates, we found that the variability of folding across individuals (and also between the left and right hemispheres of the same individual) scales with brain size and complexity of convolutions. These relationships are of interest both neurobiologically and developmentally (e.g., in relation to mechanisms of cortical folding) and from a neuroimaging methodological perspective related to the challenges of comparing data from brains that differ in shape. Examples of individual-subject and group-average data for each species are illustrated in *SI Appendix*, Fig. S1 using MRI volume slices and in *SI Appendix*, Fig. S2 using cortical surface reconstructions that represent the topology of the cortical sheet. In the macaque, individual-subject folding patterns are very similar to one another and to the group average when viewed as MRI volume slices and as cortical surface models. In addition, the left and right hemispheres are relatively symmetric by visual inspection. The bilateral symmetry of the population-average surfaces was used to generate standard-mesh representations having excellent left–right geographic correspondence (17) using GIFTI and CIFTI data formats (18). In chimpanzees, folding differences are more pronounced across individuals, and the group-average atlas surfaces (aligned using folding) show less preservation of folding detail. These differences are even more pronounced in humans, whether aligned using only cortical folding or when using areal features. The species differences between group-average surfaces are not simply a consequence of the larger number of subjects used for the human atlas ($n = 210$) vs. macaque ($n = 19$) and chimpanzee ($n = 29$) but are instead attributable to genuine species differences in folding variability (*SI Appendix*, Fig. S3).

Cortical Myelin Maps

Classical anatomists relied heavily on cytoarchitectonic and myeloarchitectonic analyses of postmortem histological data. Modern noninvasive neuroimaging has opened up new vistas for in vivo architectonics. One notably successful approach estimates myelin content based on the T1w/T2w ratio in cortical gray matter (19, 20). Fig. 2 shows cortical myelin maps for 4 primates and the mouse. In humans and macaques, these T1w/T2w–based maps are qualitatively similar to published postmortem myeloarchitectonic maps (19, 20, 22–24). Each primate species (human, chimpanzee, macaque, and marmoset) has 6 heavily myelinated regions (red and orange) that include early somatomotor (1), auditory (2), early visual (3), middle temporal (MT) complex (4), parietal (intraparietal sulcus) visual (5), and retrosplenial cortex (6). Each of these zones is surrounded by a belt of moderately myelinated cortex (yellow and green). Lightly myelinated cortex (blue and indigo) includes large swaths of cortex implicated in higher cognitive and emotion-related functions in prefrontal (A), lateral parietal (B), lateral temporal (C), medial parietal (D), and insular (E) cortex. By visual inspection, heavily myelinated regions occupy the highest portion in marmosets, lowest in humans, and intermediate in chimpanzees and macaques, as is particularly evident in the "MT+" visual region (4) and in the parietal region (5). Lightly myelinated cognitive/emotional regions show the opposite progression, being proportionally largest in humans and smallest in marmosets. These qualitative assessments are supported by quantitative measurements of the fractional size of prefrontal cortex (defined using functional as well as architectonic markers) in humans, chimpanzees, and macaques (22).

The mouse myelin map in Fig. 2 is shown on a dorsolateral view of a volumetric parcellation plus 2 coronal prefrontal sections (21). Methodological differences aside, the comparison suggests major differences between rodent and primate myelin maps. Most notably, mouse parietal cortex lacks any lightly myelinated region corresponding to primate region B. Also, lightly myelinated mouse prefrontal cortical areas ILA, ACAv, and PL (25, 26) occupy a lower percentage of cortex than primate prefrontal region A even in the marmoset.

Cortical Parcellations in Mice, Monkeys, and Humans

Cortical areas have long been considered fundamental units of cerebral cortex, but it has proven very challenging to achieve a consensus parcellation in any mammalian species. As previously noted, the many extant parcellations for humans and a variety of laboratory animals have in general been based on differences in architecture, connectivity, topography, and/or function. Most published parcellations are unimodal (e.g., purely cytoarchitectonic

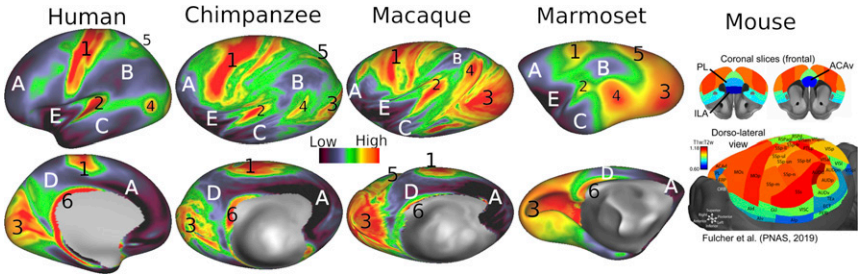

Fig. 2. Myelin maps in 5 species based on the T1w/T2w ratio. Primate data are from population-average surface-aligned data. Note that the chimpanzee and macaque surfaces are "hyperinflated" in order to reveal myelin patterns in buried regions such as the intraparietal sulcus. A single color palette applies to all 4 primates, but is scaled according to percentile ranges within each species rather than to absolute values. Mouse images are based on volumetric analysis of a single animal; adapted with permission from ref. 21. Data are available at https://balsa.wustl.edu/97vwD.

or purely resting-state functional MRI [fMRI]) and have been based on a small number of individuals (sometimes only 1 hemisphere of 1 individual). This is problematic because areal boundaries are often subtle, noisy, or inconsistent across subjects and laboratories. Confidence in a parcellation scheme is increased when multiple approaches reveal consistency in delineating areal boundaries (1, 2) and even more so when results from many individuals are accurately aligned to yield probabilistic maps that are able to illustrate individual consistency and variability.

Fig. 3 illustrates recent progress in parcellating mouse, marmoset, macaque, and human cortex, using multiple parcellations for each species. Fig. 3*A* shows 2 mouse parcellations: a 41-area parcellation (27) based on multiple immunocytochemical

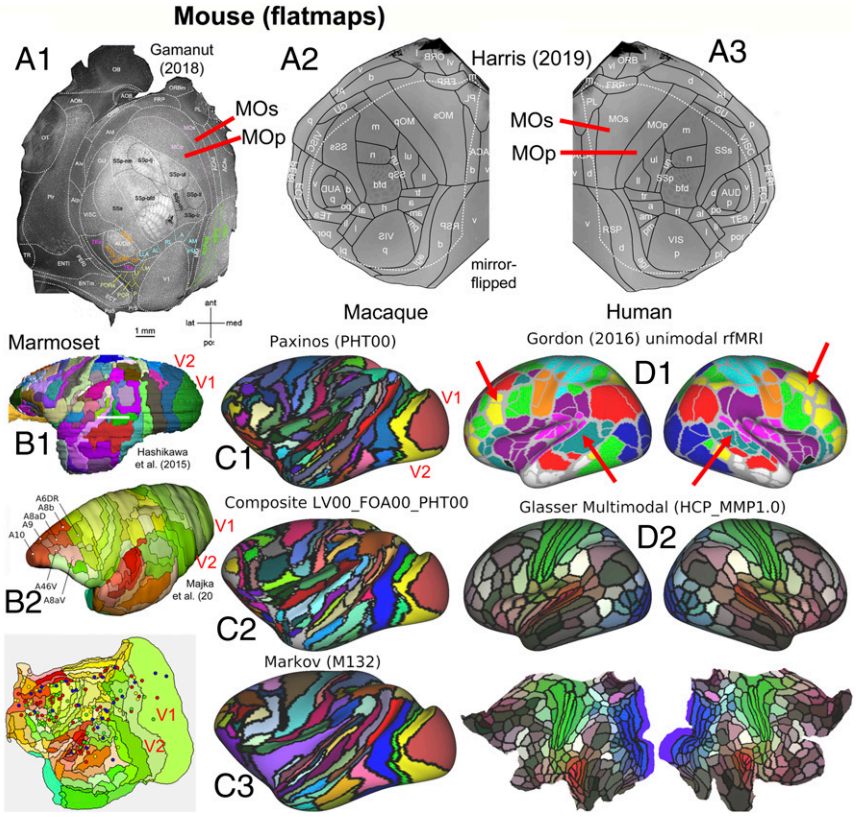

Fig. 3. Cortical parcellations in 4 species. (*A*) Two mouse parcellations. (*A1*) A 41-area parcellation of isocortical (neocortical and transitional) cortex on a flattened, tangentially sectioned left hemisphere, based on multiple immunocytochemical markers. Adapted from ref. 27, with permission from Elsevier. (*A2* and *A3*) Mouse parcellation (refs. 25 and 26; adapted with permission from ref. 26) displayed on a computationally flattened right hemisphere (*A3*) and mirror-flipped (*A2*) (symmetry assumed but not empirically demonstrated). Areal boundaries are based on numerous architectonic and immunocytochemical markers plus retinotopy using intrinsic optical imaging. Areas MOp and MOs differ in shape and relative size on the 2 flatmaps (red lines). (*B1*) Marmoset parcellation (28) is based on cytoarchitecture and multiple immunocytochemical markers. Adapted from ref. 28, with permission from Elsevier. (*B2*) Marmoset parcellation (29) is based on myelin, cytochrome oxidase, and calbindin markers. Adapted with permission from ref. 29, which is licensed under CC BY 4.0. The flatmap also shows tracer injection sites used for connectivity analyses. (*C*) Macaque cortical parcellations mapped to the Yerkes19 atlas. (*C1*) PHT00 parcellation (30) based on cytoarchitecture and SMI-32 immunocytochemistry. (*C2*) Composite multimodal parcellation (17) based on cytoarchitecture, myeloarchitecture, immunocytochemistry, and retinotopy. (*C3*) Architectonic parcellation (31) is based on cytoarchitecture and SMI-32 immunocytochemistry. (*D1*) A human unimodal parcellation (32) based on resting-state fMRI. Red arrows show pronounced asymmetric patterns in left vs. right hemispheres. (*D2*) The HCP_MMP1.0 multimodal parcellation (19) based on myelin maps, cortical thickness, resting-state fMRI, and visuotopic organization using rfMRI. Data for *C* and *D* are available at https://balsa.wustl.edu/9765g.

markers (flatmap in Fig. 3*A1*) and a 43-area isocortex parcellation (25, 26) based on many architectonic (including transgenic expression) markers, connectivity, and retinotopic mapping, displayed on a right-hemisphere flatmap (Fig. 3*A3*) and mirror-flipped in Fig. 3*A2* for easier comparison with panel A1. Both parcellations are dominated by large primary and secondary somatosensory and motor areas (SSp, SSs, MOp, MOs) plus primary visual, auditory, gustatory, and olfactory areas (V1, AUDp, GU, and Pir). In all, 37 areas are present in both schemes, and most have the same or similar names. However, there are many modest differences in size, shape, and neighborhood relationships of some of the smaller areas and even for large areas such as MOp and MOs (Fig. 3*A*, red lines), though it is unclear how much is attributable to differences in how the flatmaps were generated. Altogether, these 2 mouse schemes constitute the closest to a unified, consensus cortical parcellation to date for any species.

The most intensively studied monkeys are the marmoset and macaque (Fig. 3 *B* and *C*, respectively) and the owl monkey (2, 33). Two marmoset multimodal architectonic parcellations (28, 29) in Fig. 3 *B1* and *B2* each contain 117 cortical areas and have numerous similarities but also many differences in detail. For the macaque, there is greater divergence among widely used parcellation schemes in terms of the total number and specific arrangement of candidate areas. There are 161 areas in the PHT00 (30) cytoarchitectonic parcellation (Fig. 3*C1*), 130+ areas in the LV00_FOA00_PHT00 composite parcellation (17) (Fig. 3*C2*), and 91 areas in the Markov M132 architectonic parcellation (31).

In general, the marmoset and macaque parcellations share many commonalities and differ greatly from the mouse, which is hardly surprising in view of their evolutionary relationships. Monkeys have several-fold more areas than the mouse, along with other fundamental differences in organization. Among early sensory areas, the most prominent differences are 1) the strip-like arrangement of primate somatosensory areas (3a, 3b, 1, 2) vs. the more rounded mouse SSp and SSs, and 2) the fact that primate V1 is by far the largest primary sensory area and is nearly surrounded by a single concentric area V2 vs. the mosaic of many areas adjacent to mouse V1. In addition, monkeys have a large expanse of higher sensory, motor, and multimodal association areas in occipital, parietal, frontal, and temporal cortex that are unlikely to have strong candidate homologs in the mouse, consistent with the aforementioned observations regarding myelin maps (Fig. 2).

In humans, numerous pan-hemispheric cortical parcellation schemes have been reported, an early example being Brodmann's classic 47-area cytoarchitectonic map (34). Other studies reported many more areas, including an early myeloarchitectonic parcellation containing ~200 areas (35, 36) and triggering a century-long debate regarding the number of human cortical areas. In recent years, resting-state fMRI has been used to generate numerous unimodal but pan-hemispheric parcellations based on similarities in "functional connectivity" (correlated fluctuations in fMRI BOLD time-series data). One widely used fMRI-based parcellation (Fig. 3*D1*) contains 356 parcels in the 2 hemispheres (32). Although there are 178 parcels in each hemisphere, numerous asymmetries are evident between the left and right hemispheres (red arrows), and many parcel boundaries do not respect known visual or somatosensory-motor areal boundaries (2, 23).

Fig. 3*D2* shows the HCP_MMP1.0 multimodal group-average parcellation (23), which identified 180 areas (or area complexes) in each hemisphere by 1) using high-quality multimodal data from the Human Connectome Project (HCP); 2) processing the data to minimize artifacts, nuisance signals, distortion, and blurring; 3) accurately aligning data from hundreds of subjects to a surface-based atlas using "areal features" (not just folding patterns); 4) computing spatial gradients on group-average data for multiple modalities pertaining to architecture, connectivity, topography, and function; and 5) requiring agreement between at least 2 modalities for nearly all candidate areal borders. Importantly, the same 180 areas were identified in locations that geographically approximately correspond in the 2 hemispheres. This high degree of bilateral symmetry in human cortex (found but not forced during the parcellation process) contrasts with the numerous parcels that lack symmetric partners in Fig. 3*D1* and in many other published resting-state network (RSN)-based unimodal parcellations.

Individual Variability and Bilateral Asymmetry of Human Cortical Areas

Besides the group-average parcellation, the HCP_MMP1.0 also identified cortical areas accurately in hundreds of individual subjects, using an "areal classifier" to assign areal identity to each surface vertex in each individual by examining the 112-dimensional feature vector associated with it for characteristics matching the learned areal fingerprint (23). Here, we use the resultant individual-subject parcellations to examine variability and bilateral symmetry in 446 subjects. We previously reported (ref. 23, supplementary information, section 1.5) that each of the 180 cortical areas varies in surface area by 2-fold or more across individuals, consistent with previous reports based on fewer areas and individuals (e.g., refs. 37 and 38). Some of this apparent variability reflects "noise" in the size estimates, as evidenced by a median Dice coefficient of 0.72 for 27 test–retest subjects (who had repeat scanning sessions).

Here, we report several findings concerning parcellations in the left vs. right hemispheres (Fig. 4). 1) As shown along the vertical axis in Fig. 4*A*, the size of each area is correlated between the left and right hemispheres across individuals ($r = 0.37 \pm 0.13$; 95% CI [0.35, 0.39]). The distribution is skewed and exceeds 0.6 for 10 of the 180 areas. This correlation arises in part because total hemispheric surface area varies across individuals and is correlated between hemispheres ($r = 0.99$). After regressing out total surface area of each hemisphere as a confound, the left–right area correlation is only modestly lower ($r = 0.30 \pm 0.12$; 95% CI [0.29, 0.31]), indicating that the correlations are largely driven by factors other than total cortical extent. These observations suggest that whatever developmental and/or environmental factors determine the size of each area in each individual, there appear to be common influences in the 2 hemispheres rather than complete independence. 2) Most areas (128/180, $P < 0.05$, corrected for multiple comparisons) are significantly larger on average in 1 hemisphere compared with the other (red dots). The asymmetry index, $(L - R)/(L + R)$ (horizontal axis in Fig. 4*A*), is significant for all areas with an index greater than 0.13 in absolute value, and these span nearly the full range of left–right correlation values; it exceeds 0.2 in nearly 1/3 of all areas (57/180) and exceeds 0.4 in a few areas (6/180). Thus, many areas show a modest but potentially interesting degree of bilateral asymmetry at the level of areal size, rather than existence per se. It will also be of interest to evaluate correlations in mean cortical thickness of each area in the left vs. right hemisphere and of mean areal volume (which reflects both surface area and thickness).

An important consideration is how the left–right asymmetries and correlations shown in Fig. 4*A* vary with areal size. The coefficient of variation in area size is consistently high for small areas and declines steeply with increasing area size (Fig. 4*B*). This is consistent with the hypothesis that uncertainty (noise) in areal border delineation is similar in absolute spatial extent (millimeters distance on the cortical sheet) for both large and small areas. Similarly, the asymmetry index tends to be higher for small areas (Fig. 4*C*) but it is significant for the majority of areas across all area size ranges. Finally, the left–right correlation values tend to increase with areal size (Fig. 4*D*), but the correlation exceeds 0.4 and is significant for most areas of size greater than 500 mm^2 and for many of the smaller areas (size < 200 mm^2).

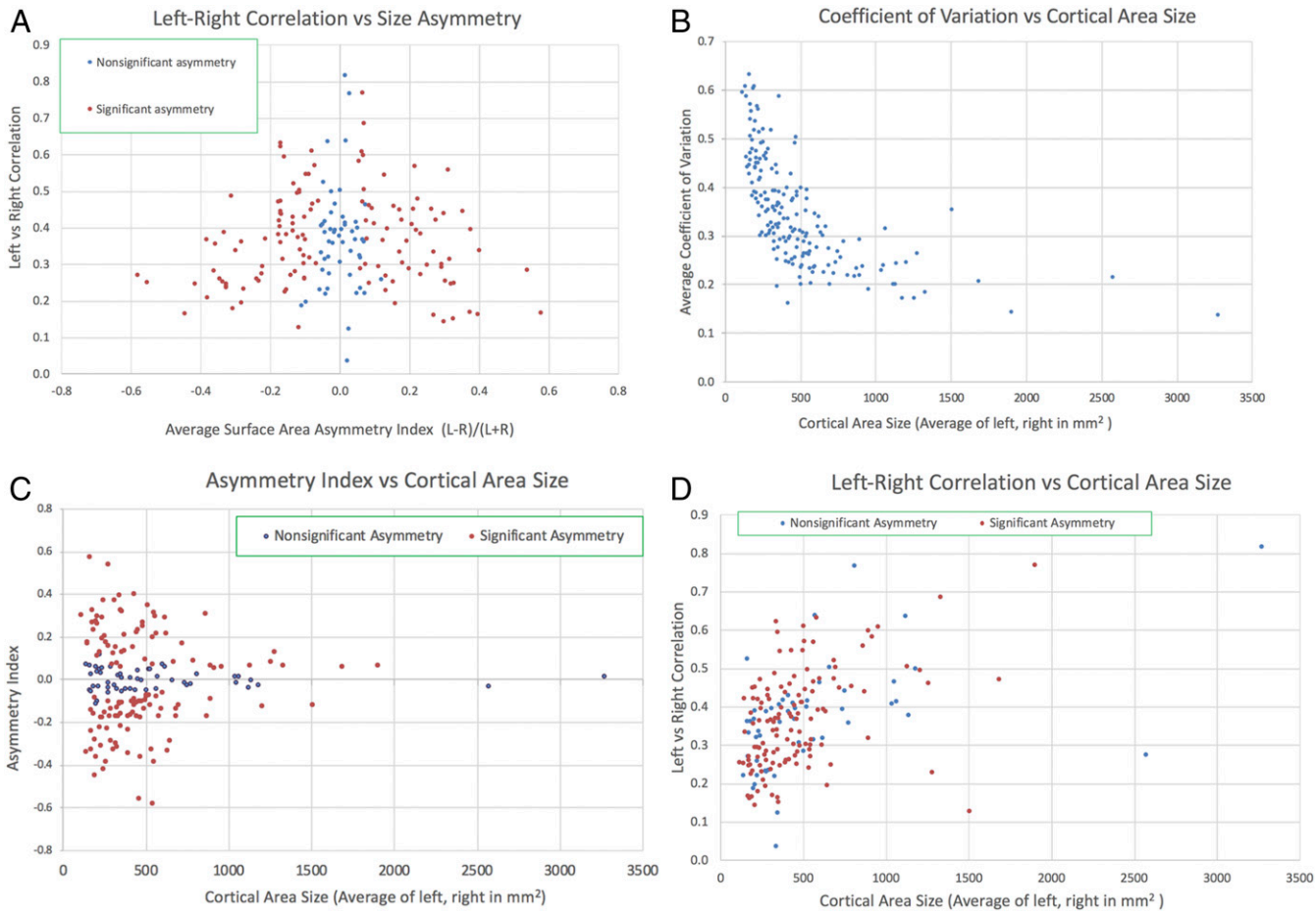

Fig. 4. Left vs. right hemisphere areal correlations and asymmetries in the human HCP_MMP1.0 cortical parcellation. (*A*) Scatterplot of an asymmetry index ([L − R]/[L + R]) on the horizontal axis, reflecting differences in the average surface area for the left vs. right hemispheres, vs. the correlation between left and right hemisphere area size (vertical axis) in 446 individual subjects (210P, 210V, plus parcellation training subjects). The small percentage of areas (4%) missing in individual subjects (23) is included in the averages. (*B*) Coefficient of variation (SD divided by the mean) for each area (computed separately for the left and right hemispheres and then averaged) as a function of mean area size (averaged across hemispheres). (*C*) The left–right average surface area asymmetry index as a function of mean area size. The 52 areas that lack significant asymmetry after multiple-comparisons correction (blue dots) all have low asymmetry indices (<0.13) but span the full range from very small to the largest cortical areas. The 128 areas having significant asymmetry fractions span nearly the full range of cortical area sizes but are weighted toward smaller areas. (*D*) Left–right correlation values vs. cortical areal size. Correlation values tend to increase with areal size, but they vary widely (several-fold or more) for all major size ranges and are comparable for areas that have significant vs. nonsignificant asymmetry fractions (red vs. blue dots).

Connectomes and Principles of Corticocortical Connectivity

Our understanding of basic principles of corticocortical connectivity has evolved dramatically over the past half-century. In the 1960s, relatively few pathways connecting relatively few areas had been identified, and an appealing conceptual framework involved the unidirectional flow of information through a serial hierarchy of visual areas (39). During the 1970s and 1980s, modern pathway-tracing methods revealed many more cortical areas and even more pathways interlinking them, including bidirectional (reciprocal) connections indicative of extensive feedforward and feedback pathways (40) and hierarchical organization (41). This led to the presentation of a distributed cortical hierarchy involving 32 visual areas at 10 discrete hierarchical levels, and an average of 10 inputs and 10 outputs for each area (1). It also included a parcellated connectivity matrix whose entries were binary (present or absent) because very little quantitative information was available at that time regarding connection weights.

In subsequent years, many additional cortical areas and corticocortical pathways have been reported, but even more important has been the ability to estimate connection weights quantitatively. This has led to the realization that corticocortical connectivity patterns are more complex in 2 important ways: 1) The number of cortical inputs and outputs to each area is typically several times larger than had previously been reported, and 2) quantitative analyses revealed that the range of connection weights is many orders of magnitude—much larger than previously believed. Fig. 5 *A* and *B* shows cortical parcellations and weighted connectivity matrices for the mouse and macaque. Fig. 5*C* illustrates a version of our current understanding of human corticocortical parcellated connectivity using resting-state fMRI.

In the mouse, an analysis of retrograde tracer injections in 19 cortical areas determined weighted connections (fraction of extrinsically labeled neurons) in each source area, including 7 subareas of SSp (27). In the resultant 19 × 47 weighted connectivity matrix (Fig. 5*A*), 97% of all possible connections that could exist were indeed identified, with a range of connection weights spanning 4 to 5 orders of magnitude. This study, plus a more recent anterograde tracer analysis involving a larger number of mouse cortical areas and also thalamic nuclei (25), builds on earlier analyses that used analogous approaches to characterize connectivity patterns in the macaque (31) and marmoset (29). In the macaque (Fig. 5*B*), a 29 × 91 connectivity matrix indicated that 66% of all possible pathways do indeed exist, with connection weights again spanning 5 orders of magnitude; for the 29 × 29

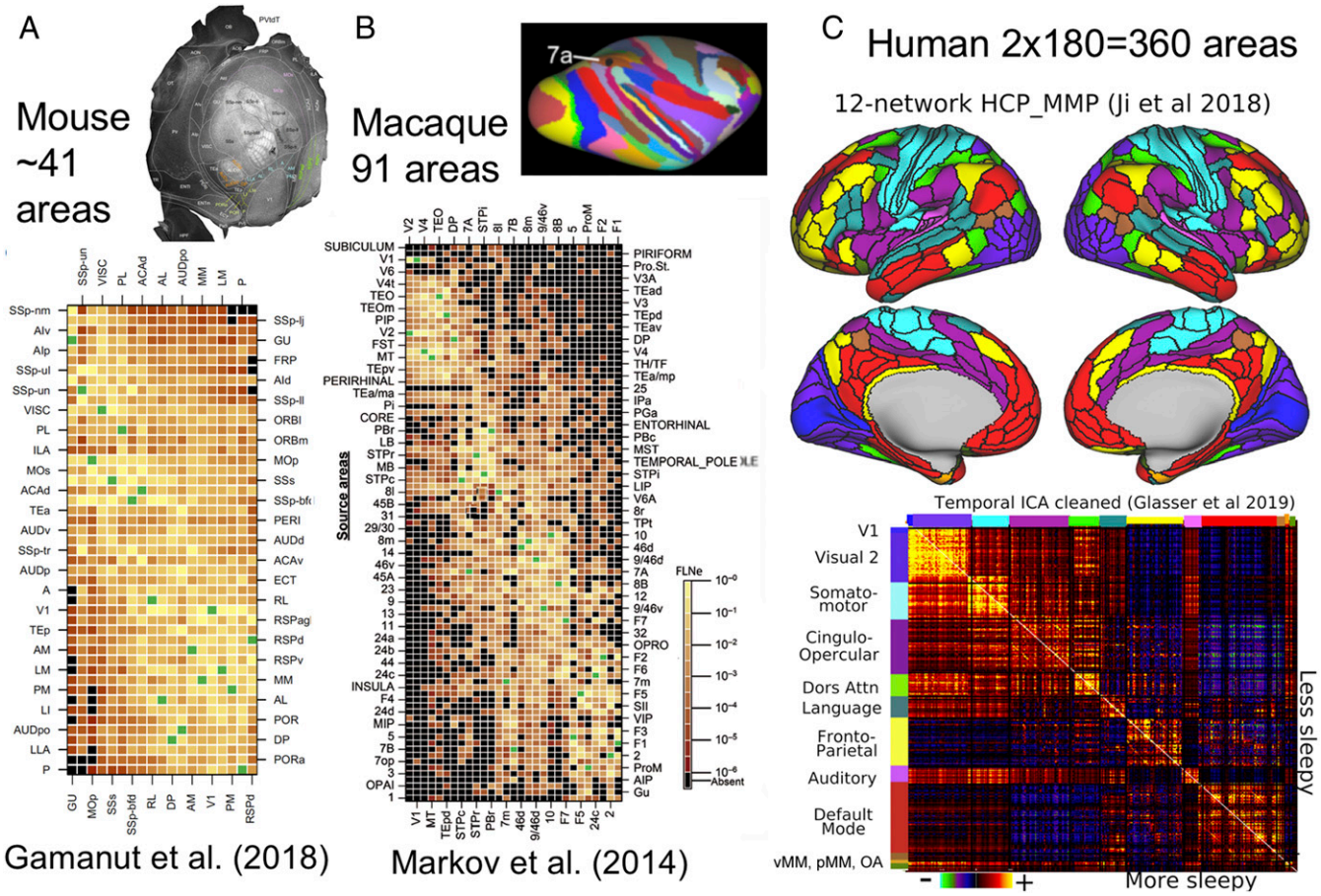

Fig. 5. Parcellated cortical connectivity matrices. (*A*) A 19 × 47 weighted connectivity matrix for the mouse, including 7 subareas of SSp. Adapted from ref. 27, with permission from Elsevier. (*B*) A 29 × 91 weighted connectivity matrix for the macaque. Adapted from ref. 31 by permission of Oxford University Press. (*C*, *Top*) A 12-network resting-state network representation of the human HCP_MMP1.0 parcellation (42). (*C*, *Bottom*) A functional connectivity matrix from 449 HCP subjects. OA, orbital affective; pMM, posterior multimodal; vMM, ventral multimodal. The published functional connectivity matrix (42) has been cleaned using tICA (43) and here shows the difference between potentially more sleepy (high mean resting-state tICA component RC1 amplitude; $n = 241$) below the diagonal and less sleepy (low mean RC1 amplitude; $n = 208$) above the diagonal, using a mean RC1 amplitude of 6 as the threshold. Data for *C* are available at https://balsa.wustl.edu/kN69P.

"edge complete graph," 2/3 of the pathways are bidirectional, and among reciprocal pathways the connection weights sometimes differ significantly (31). Similar principles appear to apply to the 55 × 117 connectivity matrix reported in the marmoset (29) (see also http://analytics.marmosetbrain.org), though many important aspects have yet to be reported in comparable detail.

An important alternative to the aforementioned notion of a cortical hierarchy having discrete processing levels involves models that represent hierarchy as a continuous variable. In the macaque, this includes a graded hierarchy scheme embedded in a feedforward and feedback counterstream organization (44, 45). In the mouse, there is evidence for a graded hierarchy involving 37 cortical areas and 24 thalamic nuclei (25) that is much shallower, involving differences in laminar patterns of inputs and outputs that are complex, sometimes subtle, and different in detail from the criteria used in the macaque. In the marmoset, current evidence for hierarchical organization (46) suggests broad similarities with the macaque, but a more detailed analysis is strongly warranted. In humans and macaques, T1w/T2w–based maps of myelin content (Fig. 2) have been proposed as a "proxy" for anatomical hierarchy that also correlates with the principal axis of transcriptional variation based on human gene expression patterns (47).

Because invasive anatomical pathway tracing is not feasible in humans, the only realistic prospects for systematically inferring long-distance connectivity come from noninvasive methods of diffusion-weighted MRI (followed by tractography to estimate "structural connectivity") and resting-state fMRI (followed by correlation analyses to estimate "functional connectivity"). Both approaches are subject to many types of error and bias (43, 48, 49); they differ in major ways from one another and from the true anatomical connectivity they aim to estimate. Fig. 5*C* shows 12 major resting-state networks identified by Ji et al. (42) based on the same HCP multimodal parcellation as in Fig. 3*D2*. This analysis provides a refined and HCP-specific representation of many networks reported in previous RSN studies (e.g., refs. 32, 50, and 51) plus several networks not previously reported of Fig. 5 *C*, *Bottom* shows a parcellated functional connectivity matrix for the 12 RSNs and 360 cortical areas, indicating high functional connectivity within each RSN and varying degrees of functional connectivity between RSNs. Negative correlations are most pronounced between the default-mode (task-negative) network (DMN) and the cinguloopercular network. Importantly, the human functional connectome illustrated here was cleaned using temporal independent-component analysis (tICA) to remove global respiratory artifacts and to show higher vs. lower estimated arousal level, respectively, above vs. below the diagonal (43, 52). The human functional connectivity matrix shows a highly distributed pattern of "connectivity" and a wide range of "connection weights" (correlation values) and in these respects appears similar to the monkey and mouse anatomical connectivity matrices. However,

functional correlations may reflect not only direct connections but also indirect anatomical pathways, common inputs, as well as other complex manifestations of neurovascular coupling, a complex and still poorly understood process (53).

Systematic, quantitative evaluations of the relationship between functional and anatomical connectivity are urgently needed in macaques and marmosets, as these are the best available animal models for addressing these issues. Initial proof of principle of this approach came a decade ago (54). Improvements in data acquisition and analysis for both modalities may lead to better strategies for inferring direct anatomical connectivity from resting-state fMRI correlations, using "ground truth" tracer-based connectivity (55).

Interspecies Surface-Based Registration

The comparisons across species described and illustrated above all involved datasets analyzed and displayed separately for each species. An attractive complementary approach involves comparisons of cortical organization after mapping between species using surface-based registration. This approach is promising to the degree that maps of cortical organization are topologically equivalent. Given the evidence discussed above for unequal numbers of cortical areas in humans (~180) vs. macaques (~140), there is unlikely to be perfect topological equivalence at the level of area-to-area correspondence. On the other hand, given the likelihood of genuine homology for many areas (especially early sensory and motor areas) and also the broad similarities in myelin maps across species (Fig. 2), there is much to be learned from exploring topology-preserving interspecies registration. Previous efforts along these lines used a landmark-based approach based on corresponding borders of areas or regions presumed to be homologous (56–58). Owing to methodological limitations (nonuniform distortions in regions between landmarks), the resultant "evolutionary expansion" maps are only rough approximations. Improvements can be anticipated using more robust algorithms (59) and stronger registration constraints (60).

Concluding Comments

In this perspective, we have discussed exciting progress in elucidating many aspects of cortical organization and connectivity in primates and rodents. On the cortical parcellation front, it is notable that in the late 20th century the macaque was widely considered to have the most detailed and accurate parcellation among any species. Over the past decade, progress in parcellation has been much greater for mouse and human cortex. Progress in the mouse has benefited from multimodal analyses that include full-hemisphere architectonics using tangential-slice postmortem histology, connectivity using tracer injections, and topographic organization and functional characterization using electrophysiology and optical methods, all done to date on a modest number of animals. The convergence of 2 independent efforts on highly similar mouse parcellations provides hope that these are approaching a consensus ground truth. For humans, the advent of MRI methods and an "HCP-style" approach to data acquisition and analysis (61) was critical in enabling the HCP_MMP1.0 parcellation in individuals as well as a group average (23). Validation using other high-quality datasets and other approaches is obviously desirable, but we emphasize the need for objective, multimodal approaches that robustly handle both false positives and false negatives in identifying genuine areal boundaries (as distinct from transitions that may reflect intraareal subparcels or overt artifacts). A high-priority future objective is to achieve consensus pan-cortical parcellations in macaques and marmosets that are based on multiple modalities. Among the various challenges is the fact that even well-defined cortical areas (e.g., V1 and MT) vary in their absolute size and also in their internal organization (33, 38, 62, 63). A robust multimodal parcellation on many subjects in a consistent spatial framework would invite a variety of intriguing questions, including some touched on here in humans (cf. Fig. 4). Progress in achieving these objectives in monkeys will depend on further improvements in data quality and data analysis.

Data Availability. Data for the study as a whole are available at https://balsa.wustl.edu/study/976M4 (64) and for individual scenes at the URLs indicated in the figure legends.

ACKNOWLEDGMENTS. Supported by Grants R01 MH-060974 (to D.C.V.E.), T32EB014855 (to C.J.D.), LABEX CORTEX (ANR-11-LABX-0042) of Université de Lyon (ANR-11-IDEX-0007) operated by the French National Research Agency (ANR) (to H.K.), ANR-11-BSV4-501, CORE-NETS (to H.K.), ANR-14-CE13-0033, ARCHI-CORE (to H.K.), ANR-15-CE32-0016, CORNET (to H.K.), Chinese Academy of Sciences President's International Fellowship Initiative Grant No. 2018VBA0011 (to H.K.), Brain/MINDS (JP18dm0207001) (to T.H.), and Brain/MINDS-beyond (JP19dm0307006) from the Japan Agency for Medical Research and Development (to T.H.). Human datasets were provided by the Human Connectome Project, WU-Minn Consortium (Principal Investigators: D.C.V.E. and Kamil Ugurbil; 1U54MH091657) funded by the 16 NIH Institutes and Centers that support the NIH Blueprint for Neuroscience Research, and by the McDonnell Center for Systems Neuroscience at Washington University.

1. D. J. Felleman, D. C. Van Essen, Distributed hierarchical processing in the primate cerebral cortex. *Cereb. Cortex* **1**, 1–47 (1991).
2. D. C. Van Essen, M. F. Glasser, Parcellating cerebral cortex: How invasive animal studies inform noninvasive mapmaking in humans. *Neuron* **99**, 640–663 (2018).
3. S. Herculano-Houzel, The human brain in numbers: A linearly scaled-up primate brain. *Front. Hum. Neurosci.* **3**, 31 (2009).
4. M. J. Benton, P. C. Donoghue, Paleontological evidence to date the tree of life. *Mol. Biol. Evol.* **24**, 26–53 (2007).
5. M. Nei, G. V. Glazko, The Wilhelmine E. Key 2001 Invitational Lecture. Estimation of divergence times for a few mammalian and several primate species. *J. Hered.* **93**, 157–164 (2002).
6. R. M. Adkins, E. L. Gelke, D. Rowe, R. L. Honeycutt, Molecular phylogeny and divergence time estimates for major rodent groups: Evidence from multiple genes. *Mol. Biol. Evol.* **18**, 777–791 (2001).
7. A. M. Cornélio, R. E. de Bittencourt-Navarrete, R. de Bittencourt Brum, C. M. Queiroz, M. R. Costa, Human brain expansion during evolution is independent of fire control and cooking. *Front. Neurosci.* **10**, 167 (2016).
8. I. F. Miller, R. A. Barton, C. L. Nunn, Quantitative uniqueness of human brain evolution revealed through phylogenetic comparative analysis. *eLife* **8**, e41250 (2019).
9. R. G. Klein, *The Human Career* (University of Chicago Press, Chicago, ed. 3, 2009).
10. B. L. Finlay, R. B. Darlington, Linked regularities in the development and evolution of mammalian brains. *Science* **268**, 1578–1584 (1995).
11. K. E. Yopak *et al*., A conserved pattern of brain scaling from sharks to primates. *Proc. Natl. Acad. Sci. U.S.A.* **107**, 12946–12951 (2010).
12. B. Mota *et al*., White matter volume and white/gray matter ratio in mammalian species as a consequence of the universal scaling of cortical folding. *Proc. Natl. Acad. Sci. U.S.A.* **116**, 15253–15261 (2019).
13. M. A. Hofman, On the evolution and geometry of the brain in mammals. *Prog. Neurobiol.* **32**, 137–158 (1989).
14. B. Mota, S. Herculano-Houzel, BRAIN STRUCTURE. Cortical folding scales universally with surface area and thickness, not number of neurons. *Science* **349**, 74–77 (2015).
15. D. C. Van Essen, "Cerebral cortical folding patterns in primates: Why they vary and what they signify" in *Evolution of Nervous Systems*, J. H. Kaas, Ed. (Academic, Oxford, 2007), pp. 267–276.
16. D. C. Van Essen, A tension-based theory of morphogenesis and compact wiring in the central nervous system. *Nature* **385**, 313–318 (1997).
17. D. C. Van Essen, M. F. Glasser, D. Dierker, J. Harwell, Cortical parcellations of the macaque monkey analyzed on surface-based atlases. *Cereb. Cortex* **22**, 2227–2240 (2012).
18. M. F. Glasser *et al*.; WU-Minn HCP Consortium, The minimal preprocessing pipelines for the Human Connectome Project. *Neuroimage* **80**, 105–124 (2013).
19. M. F. Glasser, M. S. Goyal, T. M. Preuss, M. E. Raichle, D. C. Van Essen, Trends and properties of human cerebral cortex: Correlations with cortical myelin content. *Neuroimage* **93**, 165–175 (2014).
20. M. F. Glasser, D. C. Van Essen, Mapping human cortical areas in vivo based on myelin content as revealed by T1- and T2-weighted MRI. *J. Neurosci.* **31**, 11597–11616 (2011).
21. B. D. Fulcher, J. D. Murray, V. Zerbi, X. J. Wang, Multimodal gradients across mouse cortex. Proc. Natl. Acad. Sci. U.S.A. 116, 4689–4695 (2019).
22. C. J. Donahue, M. F. Glasser, T. M. Preuss, J. K. Rilling, D. C. Van Essen, Quantitative assessment of prefrontal cortex in humans relative to nonhuman primates. *Proc. Natl. Acad. Sci. U.S.A.* **115**, E5183–E5192 (2018).
23. M. F. Glasser *et al*., A multi-modal parcellation of human cerebral cortex. *Nature* **536**, 171–178 (2016).
24. J. W. Lewis, D. C. Van Essen, Mapping of architectonic subdivisions in the macaque monkey, with emphasis on parieto-occipital cortex. *J. Comp. Neurol.* **428**, 79–111 (2000).
25. J. A. Harris *et al*., Hierarchical organization of cortical and thalamic connectivity. *Nature* **575**, 195–202 (2019).

26. J. A. Harris *et al*., The organization of intracortical connections by layer and cell class in the mouse brain. bioRxiv:10.1101/292961 (1 April 2018).
27. R. Gămănuţ *et al*., The mouse cortical connectome characterized by an ultra dense cortical graph maintains specificity by distinct connectivity profiles. *Neuron* **97**, 698–715.e10 (2018).
28. T. Hashikawa, R. Nakatomi, A. Iriki, Current models of the marmoset brain. *Neurosci. Res.* **93**, 116–127 (2015).
29. P. Majka *et al*., Towards a comprehensive atlas of cortical connections in a primate brain: Mapping tracer injection studies of the common marmoset into a reference digital template. *J. Comp. Neurol.* **524**, 2161–2181 (2016).
30. G. Paxinos, X. F. Huang, A. W. Toga, *The Rhesus Monkey Brain in Stereotaxic Coordinates* (Academic, London, 2000).
31. N. T. Markov *et al*., A weighted and directed interareal connectivity matrix for macaque cerebral cortex. *Cereb. Cortex* **24**, 17–36 (2014).
32. E. M. Gordon *et al*., Generation and evaluation of a cortical area parcellation from resting-state correlations. *Cereb. Cortex* **26**, 288–303 (2016).
33. M. I. Sereno, C. T. McDonald, J. M. Allman, Retinotopic organization of extrastriate cortex in the owl monkey—Dorsal and lateral areas. *Vis. Neurosci.* **32**, E021 (2015).
34. K. Brodmann, *Vergleichende Lokalisationslehre der Grosshirnrinde in ihren Prinzipien dargestellt auf Grund des Zellenbaues* (Barth, 1909).
35. R. Nieuwenhuys, C. A. Broere, L. Cerliani, A new myeloarchitectonic map of the human neocortex based on data from the Vogt-Vogt school. *Brain Struct. Funct.* **220**, 2551–2573 (2015).
36. C. Vogt, Allgemeinere ergebnisse unserer hirnforschung. *J. Psychol. Neurol.* **25**, 279–462 (1919).
37. K. Amunts, A. Malikovic, H. Mohlberg, T. Schormann, K. Zilles, Brodmann's areas 17 and 18 brought into stereotaxic space—Where and how variable? *Neuroimage* **11**, 66–84 (2000).
38. L. C. Sincich, D. L. Adams, J. C. Horton, Complete flatmounting of the macaque cerebral cortex. *Vis. Neurosci.* **20**, 663–686 (2003).
39. D. H. Hubel, T. N. Wiesel, Receptive fields and functional architecture in two nonstriate visual areas (18 and 19) of the cat. *J. Neurophysiol.* **28**, 229–289 (1965).
40. K. S. Rockland, D. N. Pandya, Laminar origins and terminations of cortical connections of the occipital lobe in the rhesus monkey. *Brain Res.* **179**, 3–20 (1979).
41. J. H. Maunsell, D. C. van Essen, The connections of the middle temporal visual area (MT) and their relationship to a cortical hierarchy in the macaque monkey. *J. Neurosci.* **3**, 2563–2586 (1983).
42. J. L. Ji *et al*., Mapping the human brain's cortical-subcortical functional network organization. *Neuroimage* **185**, 35–57 (2019).
43. M. F. Glasser *et al*., Using temporal ICA to selectively remove global noise while preserving global signal in functional MRI data. *Neuroimage* **181**, 692–717 (2018).
44. N. T. Markov *et al*., Cortical high-density counterstream architectures. *Science* **342**, 1238406 (2013).
45. N. T. Markov *et al*., Anatomy of hierarchy: Feedforward and feedback pathways in macaque visual cortex. *J. Comp. Neurol.* **522**, 225–259 (2014).
46. S. G. Solomon, M. G. Rosa, A simpler primate brain: The visual system of the marmoset monkey. *Front. Neural Circuits* **8**, 96 (2014).
47. J. B. Burt *et al*., Hierarchy of transcriptomic specialization across human cortex captured by structural neuroimaging topography. *Nat. Neurosci.* **21**, 1251–1259 (2018).
48. C. Reveley *et al*., Superficial white matter fiber systems impede detection of long-range cortical connections in diffusion MR tractography. *Proc. Natl. Acad. Sci. U.S.A.* **112**, E2820–E2828 (2015).
49. C. J. Donahue *et al*., Using diffusion tractography to predict cortical connection strength and distance: A quantitative comparison with tracers in the monkey. *J. Neurosci.* **36**, 6758–6770 (2016).
50. J. D. Power *et al*., Functional network organization of the human brain. *Neuron* **72**, 665–678 (2011).
51. B. T. Yeo *et al*., The organization of the human cerebral cortex estimated by intrinsic functional connectivity. *J. Neurophysiol.* **106**, 1125–1165 (2011).
52. M. F. Glasser *et al*., Classification of temporal ICA components for separating global noise from fMRI data: Reply to Power. *Neuroimage* **197**, 435–438 (2019).
53. C. Iadecola, The neurovascular unit coming of age: A journey through neurovascular coupling in health and disease. *Neuron* **96**, 17–42 (2017).
54. J. L. Vincent *et al*., Intrinsic functional architecture in the anaesthetized monkey brain. *Nature* **447**, 83–86 (2007).
55. Y. Hori *et al*., Comparison of resting-state functional connectivity in marmosets with tracer-based cellular connectivity. *Neuroimage* **204**, 116241 (2019).
56. T. A. Chaplin, H. H. Yu, J. G. Soares, R. Gattass, M. G. Rosa, A conserved pattern of differential expansion of cortical areas in simian primates. *J. Neurosci.* **33**, 15120–15125 (2013).
57. G. A. Orban, D. Van Essen, W. Vanduffel, Comparative mapping of higher visual areas in monkeys and humans. *Trends Cogn. Sci.* **8**, 315–324 (2004).
58. D. C. Van Essen, D. L. Dierker, Surface-based and probabilistic atlases of primate cerebral cortex. *Neuron* **56**, 209–225 (2007).
59. E. C. Robinson *et al*., Multimodal surface matching with higher-order smoothness constraints. *Neuroimage* **167**, 453–465 (2018).
60. T. Xu *et al*., Cross-species functional alignment reveals evolutionary hierarchy within the connectome. bioRxiv:10.1101/692616 (4 July 2019).
61. M. F. Glasser *et al*., The Human Connectome Project's neuroimaging approach. *Nat. Neurosci.* **19**, 1175–1187 (2016).
62. J. H. Maunsell, D. C. Van Essen, Topographic organization of the middle temporal visual area in the macaque monkey: Representational biases and the relationship to callosal connections and myeloarchitectonic boundaries. *J. Comp. Neurol.* **266**, 535–555 (1987).
63. Q. Zhu, W. Vanduffel, Submillimeter fMRI reveals a layout of dorsal visual cortex in macaques, remarkably similar to New World monkeys. *Proc. Natl. Acad. Sci. U.S.A.* **116**, 2306–2311 (2019).
64. D. C. Van Essen *et al*., Cerebral cortical folding, parcellation, and connectivity in humans, nonhuman primates, and mice. BALSA. https://balsa.wustl.edu/study/976M4. Deposited 25 August 2019.